



# Discontinuous surface cracks during stress corrosion cracking of stainless steel single crystal

L.J. Qiao<sup>a,\*</sup>, K.W. Gao<sup>a</sup>, Alex A. Volinsky<sup>a,b</sup>, X.Y. Li<sup>c</sup>

<sup>a</sup> Department of Materials Physics, Corrosion and Protection Center, Key Laboratory for Environmental Fracture (MOE), University of Science and Technology Beijing, Beijing 100083, People's Republic of China

<sup>b</sup> Department of Mechanical Engineering, University of South Florida, 4202 E. Fowler Ave. ENB118, Tampa, FL 33620, USA

<sup>c</sup> Jinzhou Petrochemical Corporation, China National Petroleum Corporation, Jinzhou, Liaoning 121001, People's Republic of China

## ARTICLE INFO

### Article history:

Received 27 March 2011

Accepted 16 June 2011

Available online 23 June 2011

### Keywords:

A. Stainless steel

B. SEM

C. Stress corrosion

## ABSTRACT

Single crystal 321 stainless steel stress corrosion cracking was studied in a 42 wt.% MgCl<sub>2</sub> solution. Cracks propagated macroscopically in the maximum tensile stress plane regardless of the notch orientation with respect to the applied tensile load direction. Some stress corrosion cracks nucleated discontinuously at the intersection of the two slip bands. Most cracks, however, were not related to the slip bands. Cleavage-like fracture was observed, and the river-markings exhibited microshear facets along the {1 1 1} plane. Interaction between the main crack and the discontinuous microcracks increased the calculated stress intensity factor by 17 times and promoted crack coalescence, resulting in mechanical fracture of the ligaments between the cracks.

© 2011 Elsevier Ltd. All rights reserved.

## 1. Introduction

Metal deformation and fracture in solutions have been studied for many years, but, until now, the exact mechanisms have not been clearly explained. Recently many investigators focused on studying single crystals because of their simple structure as compared with polycrystalline materials. Different testing methods [1–5] and environments [6–10] were often used as variable parameters with special consideration given to the angle between the direction of the applied load and the crystal orientation [11–17].

In face centered cubic (FCC) materials, dislocations often pile up at the Lomer-Cottrell sessile dislocations. Dislocation pile-ups enhance the local electrochemical activation of these locks, initiating the microcracks. After microcrack initiation, dislocations continue to pile up around the crack tip, causing stress concentrations. When the stress intensity factor,  $K_I$ , ahead of the crack tip becomes equal to the fracture toughness,  $K_{IC}$ , the crack will open and propagate. Stroh showed that in FCC materials, the number of dislocations required to initiate a crack at the Lomer-Cottrell locks, just by shear, was roughly an order of magnitude less than that required for actually opening up a crack [18]. Therefore, the fracture of most FCC metals is ductile. The chemical environment changes  $K_{IC}$  and the critical shear stress. Therefore, it is possible for FCC metals to undergo brittle fracture. Mimaki performed stress corrosion cracking (SCC) tests on copper bicrystals with  $\langle 1 1 0 \rangle$ -tilt  $\Sigma 3$ ,

$\Sigma 9$ , and  $\Sigma 11$  coincident site lattice boundaries [19]. For the three types of specimen, it was found that many cracks initiated on the side surface, at the sites where the two slip systems intersected with each other along the {1 1 0} trace and perpendicular to the applied stress axis. During SCC of oriented copper–zinc single crystals, under various chemical conditions, fracture surfaces were predominantly {1 1 0}, independent of the tensile axis orientation, and had occasional appearances of the {1 1 1} fracture planes [8]. Meletis and Hochman [20] also proposed that, in copper single crystals, dislocations moving on two intersecting {1 1 1} slip systems can combine to produce  $\langle 1 1 0 \rangle$  sessile Lomer-Cottrell dislocations. Based on detailed microfractography of transgranular SCC in 316 and 310 stainless steels (SS), tested in a boiling MgCl<sub>2</sub> solution, Dickson et al. [21] and Magnin [22] reported that localized slip of the {1 1 1} planes induced cleavage. The {1 1 1} facets are often small and their size increases by increasing the  $K_I$  stress intensity factor.

Despite a considerable amount of research, conflicting views on SCC mechanisms remain. Several models have been proposed to explain transgranular crack propagation via discontinuous cleavage [8,22–25]. A film-induced cleavage model has been developed and was based on the work with Cu–Au and Cu–Zn alloys [24]. Microcleavage is induced in the ductile matrix by the brittle cracking of the surface layer, which is strongly affected by hydrogen [26]. Two other models, involving micro-cleavage due to dislocation pile-up, were proposed [8,22,23,25,27]. One was based on the influence of localized anodic dissolution upon the plasticity enhancement at the crack tip [22,23,25]. This localized plasticity

\* Corresponding author. Tel.: +86 10 6233 4499; fax: +86 10 6233 2345.

E-mail address: [lqiao@ustb.edu.cn](mailto:lqiao@ustb.edu.cn) (L.J. Qiao).

enhancement leads to the formation of dislocation pile-ups, where Lomer-Cottrell barriers, or other obstacles, occur. Microcleavage, and/or microshear, is induced by the restricted slip conditions, resulting in brittle transgranular microcracking. Crack propagation is then limited and arrested by the strong relaxation effects in the intrinsically ductile 316 stainless steel. The other model was based on the anodic dissolution effect upon fracture toughness,  $K_{IC}$  [8,27]. The model incorporates Stroh's pile-up mechanism for opening up a Lomer-Cottrell lock, but the stress state at the lock is modified by a corrosion process occurring at the main crack tip [18]. The nucleated crack grows as a result of a "burst" of pile-up dislocations flowing into the fractured lock. Blunting of this crack is initially prevented because the stress state at the crack nucleus is not sufficient to activate appropriate slip and because the time available for the activation of such slip is limited. It is postulated that continued growth is controlled by the effect of selective dissolution upon  $K_{IC}$  at the crack tip and is not simply due to Faraday dissolution. Subsequent blunting depends on the direction of the crack growth and the crack tip dissolution rate.

Most models proposed in the literature assume that the role of stress is to induce slip emergence on a specimen surface. The slip emergence and anodic dissolution are regarded as separate steps. The synergistic action of stress and anodic dissolution is neglected. This paper aims to investigate the initiation, propagation and coalescence of stress corrosion cracks, while also considering the effect of stress on anodic dissolution and investigating the crystalline planes of a 321 stainless steel single crystal cracking surface.

## 2. Experimental procedure

321 SS single crystals were used in this study. The crystals were produced along the  $[0\ 1\ 0]$  direction with the following chemical composition: C–0.06 wt.%, Cr–18.7 wt.%, Ni–9.87 wt.%, Mn–1.8 wt.%, Si–1 wt.%, Ti–0.45 wt.%, Fe–balance. The crystals were machined into notched specimens with  $50 \times 10 \times 0.15\text{ mm}^3$  dimensions and the notch configuration shown in Fig. 1. Samples were annealed at  $1050\text{ }^\circ\text{C}$  for 30 min in argon and then air cooled. The notch tip radius was 0.15 mm. Specimen side surfaces coincide with  $\{1\ 0\ 0\}$  planes. The specimen is under mode I, or mixed mode I + II loading, when the load is applied along the  $[0\ 1\ 0]$  long axis direction. All specimens were mechanically polished. SCC tests were performed in a 42 wt.%  $\text{MgCl}_2$  boiling solution ( $143\text{ }^\circ\text{C}$ ) at corrosion potential and under constant load. After the tests, each specimen was ultrasonically cleaned; first in hot water and then in a 5 wt.% HCl + 2 g/L hexamethylenetetramine mixture. The fractography and slip bands of the cracked specimens were observed using scanning electron microscopy (SEM).

## 3. Results

### 3.1. Macroscopic SCC propagation

The specimens were strained under pure mode I and mixed mode I + II loading. SCC propagation under mode I loading is shown in Fig. 2a, where the specimen was loaded with 48 MPa nominal stress for 6 h. The arrows indicate the loading direction. The main crack is macroscopically perpendicular to the applied load direc-

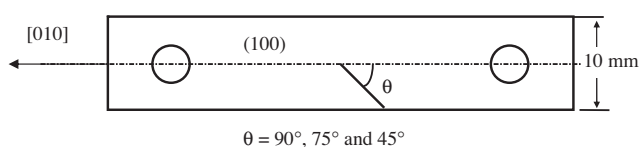


Fig. 1. Schematics of the stainless steel single crystal mixed mode I + II specimen.

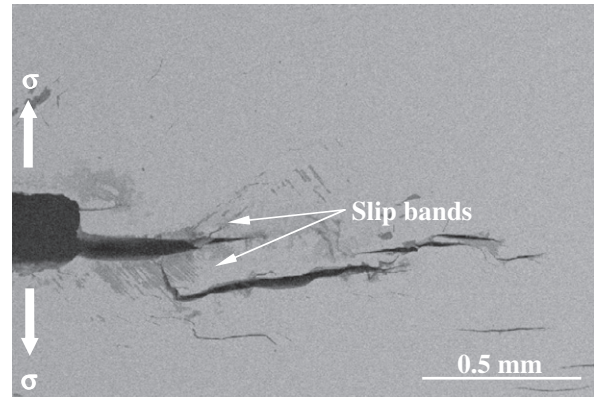


Fig. 2a. SCC and slip bands under pure mode I loading with 48 MPa stress in 42 wt.%  $\text{MgCl}_2$  boiling solution for 6 h.

tion. Some discontinuous cracks are also perpendicular to the loading direction, except for the connecting part. No slip band can be found around the discontinuous cracks, but two groups of slip bands exist on both sides of the main crack, intersecting the main crack at a  $45^\circ$  angle.  $\{1\ 1\ 1\}$  slip lines have  $45^\circ$  directions in  $\{1\ 0\ 0\}$  planes and the intersection angle between  $\{1\ 1\ 1\}$  and  $\{1\ 0\ 0\}$  planes is  $90^\circ$ .  $\{1\ 0\ 0\}$  are the only planes whose  $\{1\ 1\ 1\}$  slip lines can intersect at  $90^\circ$  angle. Therefore, the slip bands are from  $\{1\ 1\ 1\}$  planes and the main crack is in the  $(100)$  plane according to the FCC crystal orientation.

For the mixed mode I + II specimens ( $\theta = 45^\circ$ ), the results of SCC are similar to that of the mode I specimens. Fig. 2b shows SCC propagation direction in the specimen loaded with 119 MPa nominal stress. The time to fracture was 4 h. Similar to mode I loading (Fig. 2a), the crack propagation is perpendicular to the loading direction. Many cracks are parallel to the main crack. There are also perpendicular slip lines on the side surface, in the cracked area. There were many more slip bands in Fig. 2b because of the higher stress level. No relationship can be found between the slip lines and the crack direction. For specimens with  $\theta = 75^\circ$ , cracks also propagated in the plane perpendicular to the loading direction. A previous study showed that pure mode II SCC also initiated at the maximum normal stress site and propagated along the maximum stress direction. There were no slip lines adjacent to the crack [15].

At lower stress levels, stress corrosion cracks could propagate a long distance without slip lines appearing. Fig. 3 shows the low

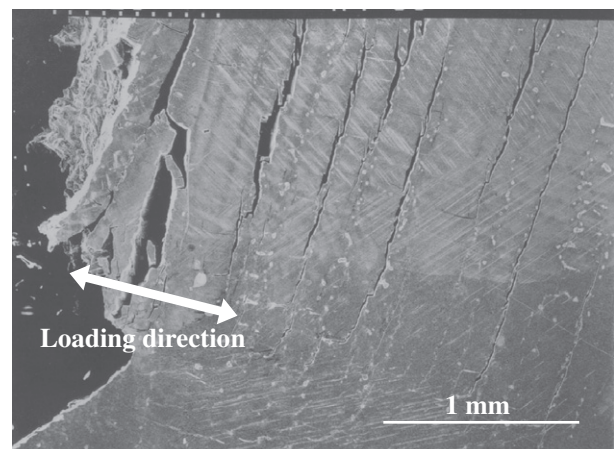
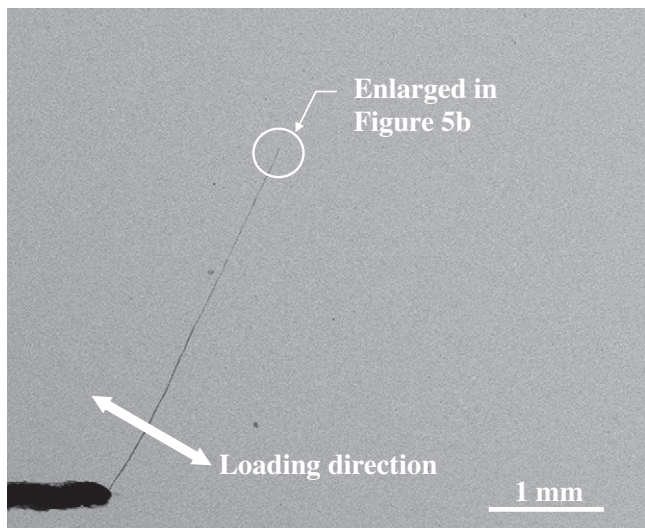


Fig. 2b. SCC and slip bands under mixed mode I + II ( $\theta = 45^\circ$ ) loading with 119 MPa stress.



**Fig. 3.** SCC without any slip bands under mixed mode I + II ( $\theta = 45^\circ$ ) loading with 27 MPa stress.

stress example (mode I + II,  $\theta = 45^\circ$ ), in which less than 27 MPa of nominal stress was applied for 13 h. The crack is perpendicular to the applied loading direction and is not associated with any of the slip bands. Mode I, II, and mixed mode I + II loading showed that stress corrosion cracks always propagate macroscopically in the direction perpendicular to the normal stress.

### 3.2. Microcrack initiation and propagation

Stress corrosion crack initiation and propagation may or may not be associated with slip bands, according to the above results. To clarify this, microcrack initiation and propagation were characterized. Fig. 4a shows microcrack initiation on intersection sites of two groups of  $\{1\ 1\ 1\}$  slip bands in the  $(0\ 0\ 1)$  plane. The slip lines are perpendicular to each other and some of them corroded. Details of corroded slip bands are shown in Fig. 4b. Corrosion occurred along the crystalline planes, but did not form microcracks. The specimen was loaded with 66 MPa stress for 220 min along the  $[0\ 1\ 0]$  direction. Therefore, microcracks propagated in the  $(0\ 1\ 0)$  plane, perpendicular to the loading direction. Fig. 5a shows corroded slip bands in the specimen presented in Fig. 2b. Slip lines,

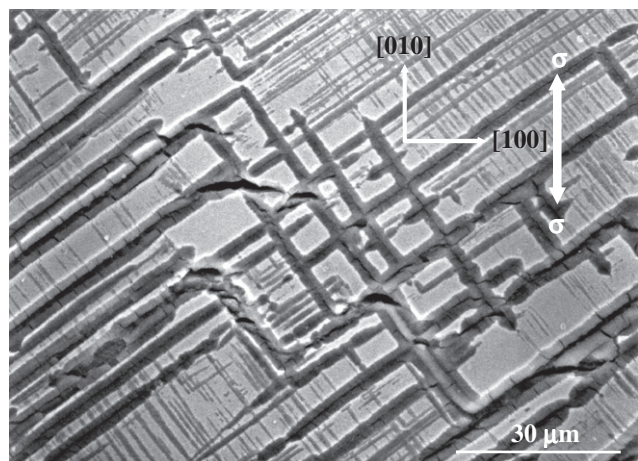


**Fig. 4a.** Initiation of discontinuous micro-cracks on the  $(1\ 0\ 0)$  plane at intersection sites of slip bands from  $(1\ 1\ 1)$  planes.

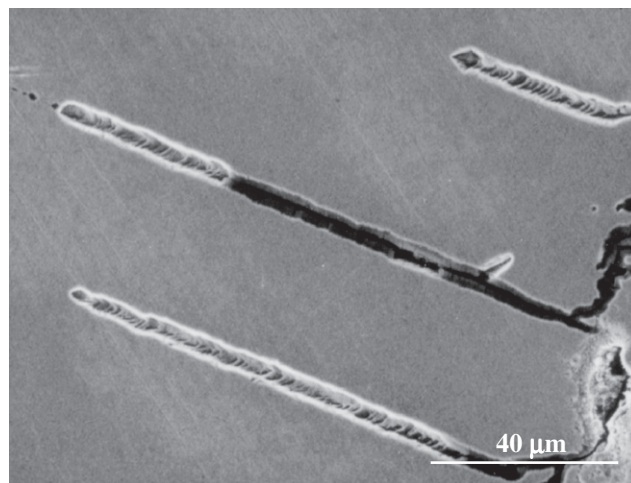


**Fig. 4b.** Corroded slip bands.

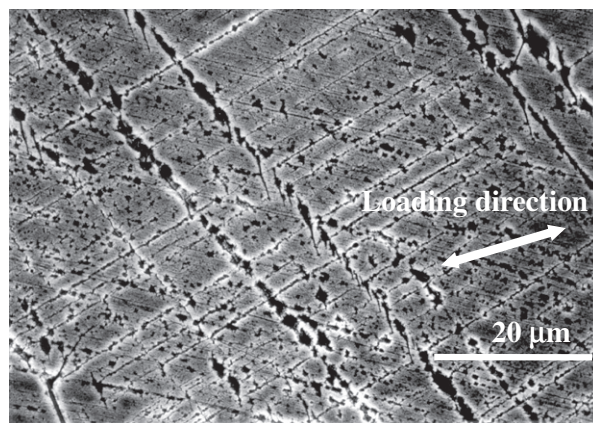


**Fig. 5a.** Multi-initiation and propagation of angled micro-cracks on the slip bands.

almost perpendicular to the loading direction, corroded heavily, with many initiated microcracks as compared with slip lines almost parallel to the loading direction. However, the microcracks are inclined and are not directed along the slip lines. They are

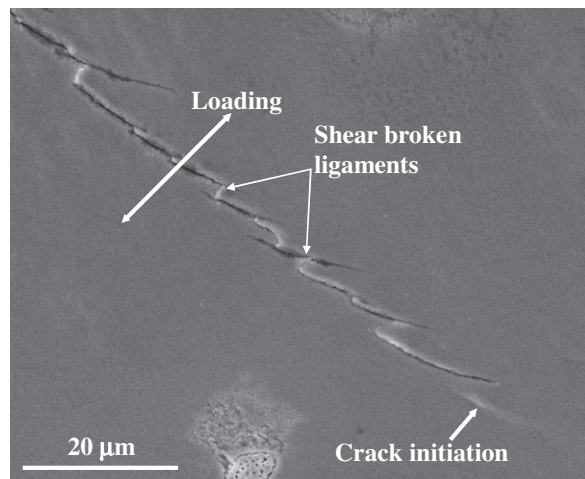


**Fig. 5b.** Initiation of discontinuous micro-cracks and microcrack coalescence with the main crack.

perpendicular to the normal stress planes. No microcracks formed in other slip bands, forming a small angle with the applied stress direction. Figs. 5 and 6 indicate that cracking is not related to the slip band formation. The slip bands are probably the result of high stress and merely accompany SCC. SCC can occur without any slip bands, as shown in Fig. 5b, which presents the crack tip of the specimen shown in Fig. 3. It can be seen that cracks initiated discontinuously and then connected with each other through breaking of the ligaments between the main crack and the microcracks. The last microcrack just initiated and is not connected with the previous one yet, as indicated by an arrow.

### 3.3. Cracking plane

The above results showed that SCC could occur with and without appearance of the slip bands. However, fracture surfaces of SCC generally exhibit highly crystallographic cleavage or cleavage-like features. Fig. 6a shows a configuration of the cracking surface and the crystallographic plane. The lower-left part is the side surface of the specimen. There are many parallel lines which are slip bands from {1 1 1} slip planes. The upper-right part is a typical fracture surface observed in many SCC situations. There are many stepped cleavage planes on the SCC surface. Stepped cleavage planes compose river or fan patterns on the SCC surface of stainless

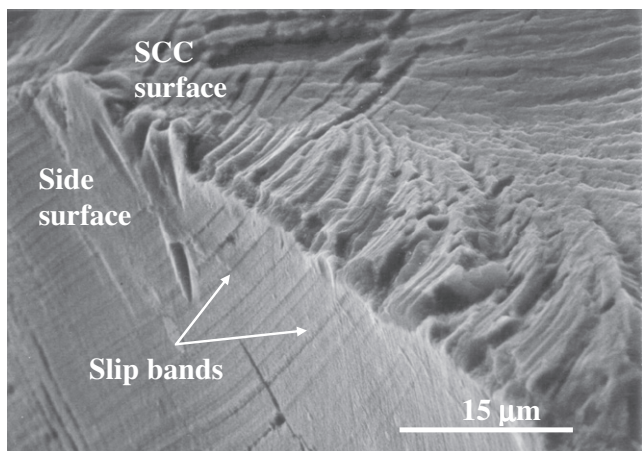


Fig. 6a. Configuration of cracking planes on the SCC surface and slip bands on the side surface: the cracking planes located on the same planes as dislocation slip bands.

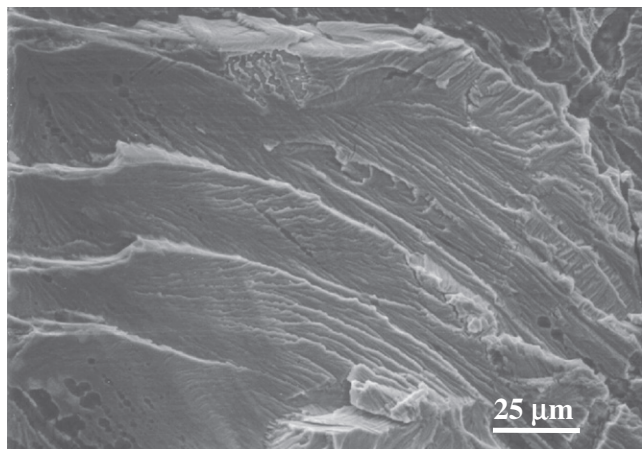


Fig. 6b. Most often observed SCC morphology of stainless steels in 42 wt.% MgCl<sub>2</sub> boiling solution.

steels in many situations, as shown in Fig. 6b. It can be seen from Fig. 6a that the stepped cleavage planes are located in the same dislocation slip planes, i.e., the cleavage surfaces are {1 1 1} planes. This is consistent with other results. Magnin et al. [22,27–29] analyzed cracking using the corrosion-enhanced plasticity model. The authors pointed out that {1 0 0} and {1 1 0} planes formed by microcracking of the {1 1 1} planes, in a zigzag manner.

## 4. Discussion

### 4.1. Discontinuous crack initiation

For an elastic material, the stress distribution can be calculated using linear elastic fracture mechanics with the maximum stress located at the crack tip. As a result, the crack propagates directly from the crack tip. The stress distribution in front of the crack can be calculated approximately using linear elastic fracture mechanics. The stresses in front of the crack tip are [30]:

$$\sigma_x = \frac{K_I}{\sqrt{2\pi r}} \left[ \cos \frac{\theta}{2} \left( 1 - \sin \frac{\theta}{2} \sin \frac{3\theta}{2} \right) \right] \quad (1)$$

$$\sigma_y = \frac{K_I}{\sqrt{2\pi r}} \left[ \cos \frac{\theta}{2} \left( 1 + \sin \frac{\theta}{2} \sin \frac{3\theta}{2} \right) \right] \quad (2)$$

$$\sigma_{\max} = \frac{K_I}{\sqrt{2\pi r}} \left[ \cos \left( \frac{\theta}{2} \right) \left( 1 + \sin \left( \frac{\theta}{2} \right) \right) \right] \quad (3)$$

However, the situation is different when plastic deformation takes place. Similar to confined ductile thin film geometry [31], maximum stress is no longer at the crack tip if dislocations are emitted from the crack tip because of the dislocations' shielding stress. The shielding effect causes the maximum stress position to shift away from the main crack tip [32]. A highly stressed zone forms ahead of the crack tip in the case of plastic deformation. The shift distance depends on the level of the applied  $K_I$  [33]. A shifted and highly concentrated normal stress could result in discontinuous initiation of the microcrack [34]. The distribution of dislocations, the normal stress and a discontinuous microcrack in front of the main crack are shown schematically in Fig. 7a.

The slip emergence and anodic dissolution are regarded as two separate steps in most anodic dissolution models. The synergistic action of the stress and anodic dissolution were neglected in previous slip-dissolution models. In fact, dislocations play two roles in SCC. First, dislocations generate slip steps, disrupting the surface protective film. As a result, freshly exposed metal is subjected to corrosion. Second, dislocations pile-up, resulting in highly localized stress, which cause atoms to dissolve preferentially. Only the first

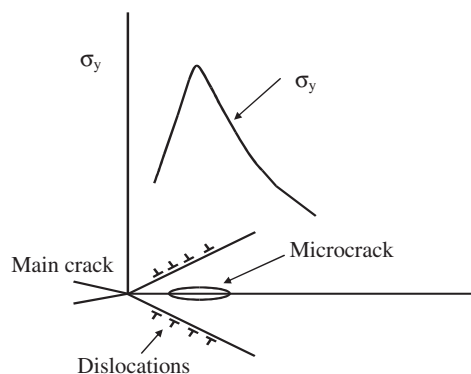


Fig. 7a. Schematics of dislocations distribution, normal stress and discontinuous microcrack in front of the main crack.

role of stress is considered in most SCC models in the literature. Synergistic effects of stress and chemical medium should be taken into account to explain the mechanism. The effect of stress on anodic dissolution current can be expressed as follows [35]:

$$i(\sigma) = i_A \cdot \exp\left(\frac{M\sigma^2}{2E\rho RT}\right) \quad (4)$$

where  $M$  is the atomic weight,  $\sigma$  is the applied stress,  $E$  is the Young's modulus,  $\rho$  is the density,  $R$  is the gas constant,  $T$  is the absolute temperature,  $i(\sigma)$  and  $i_A$  are anodic currents with and without the applied stress,  $\sigma$ , respectively. Elastic stress in bulk specimens is typically small and has little effect on anodic dissolution, based on Eq. (4). The local stress around the tip of a dislocation pile-up, however, could reach the theoretical cohesive strength. For stainless steels, Young's modulus  $E$  is about 200 GPa. Substituting  $\sigma = 0.1 E = 20$  GPa,  $M = 56$  g/mol and  $R = 8.31$  J/mol into Eq. (6) yields  $i(\sigma) = 18i_A$  for  $T = 298$  K. The effect of highly localized stress on the anodic process plays a critical role in SCC.

Dislocations could pile up against various obstacles, such as sessile dislocations, surface films, inclusions and interfaces. Such pile-ups at different obstacles may result in different cracking behaviors. For instance, pile-up against grain boundaries probably results in intergranular cracks. The pile-up against surface film or obstacles in grains will result in transgranular cracks. For austenitic stainless steel, the slip system is  $\{111\}$ – $\langle 110 \rangle$ . Dislocations gliding on  $\{111\}$  planes will form a Lomer-Cottrell sessile dislocation in the  $\{110\}$  planes. Dislocation pile-up against the Lomer-Cottrell barrier results in a highly localized stress concentration, which forms a local high stress region. Discontinuous microcracks will initiate in the high stress zone ahead of the main crack, as observed in Fig. 5b. Dislocation slip on different planes with the same direction may result in many parallel Lomer-Cottrell sessile dislocations, consequently resulting in multiple microcracks nucleating on the slip band, as illustrated in Fig. 7b. This situation is consistent with the observed result in Fig. 5a. Dislocation pile-up against the surface film results in the slip bands and crack planes seen in Fig. 6a.

Stress corrosion cracks can initiate and propagate without any slip bands if the applied stress is low, as seen in Figs. 3 and 5b.

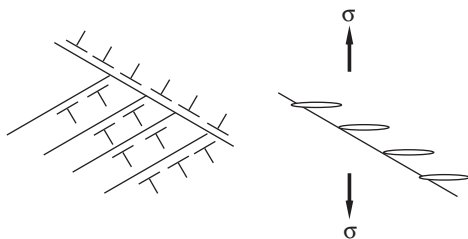


Fig. 7b. Schematics of multi-slip systems and discontinuous microcracks.

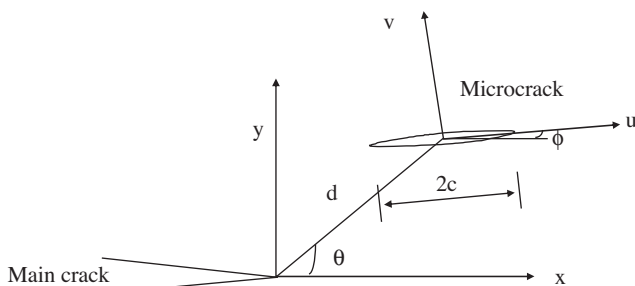


Fig. 7c. Configuration of the main crack and the micro-crack under mode I loading.

Although microcracks can occur on slip bands for the case of a high stress level, the cracking direction is inclined to the slip bands. This is not consistent with the “slip-dissolution” model prediction. Dislocations play an important role in the SCC process via slip and pile-up at particular obstacles, resulting in high local stress. The slip bands were just an accompanying result at a high stress level and, consequently, did not contribute directly to the SCC process.

#### 4.2. Coalescence of discontinuous microcracks with the main crack

The stress intensity factor at the main crack tip is amplified when a discontinuous microcrack initiates ahead of the main crack tip. For an arbitrarily located and oriented microcrack under mode I loading, as shown in Fig. 7c, the stress intensity factor  $K_I^M$  of the main crack can be written as [36]:

$$K_I^M = K_I \left[ 1 + \alpha \left( \frac{c}{8d} \right)^2 \right] \quad (5)$$

where  $c$  is the half length of the microcrack,  $d$  is the distance from the main crack tip to the center of the microcrack, and

$$\alpha = 2 \cos(2\phi + \theta) + 4 \cos(2\phi - \theta) + 8(2\phi - 2\theta) - 6 \cos(2\phi - 3\theta) - 8 \cos(2\phi - 4\theta) - 3 \cos(3\theta) + 8 \cos(2\theta) + 11 \cos(\theta) \quad (6)$$

where  $\theta$  is the location angle and  $\phi$  is the microcrack orientation angle, as indicated in Fig. 7c.

A microcrack could either shield or enhance the stress intensity factor at the main crack tip based on the  $\phi$  and  $\theta$  angles values. When the microcrack is collinear with the main crack ( $\theta = 0$ ),  $\alpha$  is 16 and does not depend on the microcrack orientation angle  $\phi$ . The maximum value of  $\alpha$  could reach 28. The  $c/d$  ratio is about 3–6, as shown in Fig. 5b. The stress intensity factor of the main crack could be increased up to 17 times by the discontinuous microcracks. The increased stress intensity factor facilitates crack coalesce at a lower applied stress level.

## 5. Conclusions

- (1) Stress corrosion cracks in stainless steel single crystals propagated in the normal stress planes for all notch orientations.
- (2) Stress corrosion cracks can initiate and propagate without any slip bands.
- (3) For the case of a high stress level, slip bands appeared on the surface with many microcracks present on the slip bands themselves. The microcrack direction is not along the slip bands. Instead, microcracks are aligned with the tensile stress plane.
- (4) The main crack interaction with discontinuous microcracks enhanced the effective stress intensity factor and facilitated crack propagation.

## Acknowledgements

This research was supported by the National Natural Science Foundation of China (50731003 and 10776001) and Beijing Municipal Science and Technology Commission (D09030303790901). Alex Volinsky acknowledges support from the National Science Foundation.

## References

- [1] S.X. Li, D.J. Smith, Modelling of anisotropic creep deformation and damage in single crystal superalloys, *Scripta Metall. Mater.* 33 (1995) 711–718.
- [2] B.F. Antolovich, A. Saxena, S.D. Antolovich, Fatigue crack propagation in single-crystal CMSX-2 at elevated temperature, *J. Mater. Eng. Perfor.* 2 (1993) 489–496.

- [3] H. Koizumi, S. Katakura, T. Suzuki, Crack propagation velocity in NaCl single crystals, *Mater. Sci. Eng.* A176 (1994) 417–420.
- [4] H. Uchida, M. Yamashita, S. Inoue, K. Koterazawa, In-situ observations of crack nucleation and growth during stress corrosion by scanning vibrating electrode technique, *Mater. Sci. Eng.* A319–321 (2001) 496–500.
- [5] D.E. Kramer, M.F. Savage, L.E. Levine, AFM observations of slip band development in Al single crystals, *Acta Mater.* 53 (2005) 4655–4664.
- [6] K. Koterazawa, H. Uchida, T. Nonomura, Tensile orientation dependence of hydrogen embrittlement in SUS304 stainless steel single crystals, *J. Soc. Mater. Sci.* 43 (1994) 867–873.
- [7] K. Kitajima, Modelling of hydrogen-induced fracture in iron, *Mater. Sci. Eng.* A 176 (1994) 249–253.
- [8] B.D. Lichter, W.F. Flanagan, J.S. Kim, J.C. Elkenbracht, M. Van Hunen, Mechanistic studies of stress corrosion cracking: application of the corrosion-assisted cleavage model to results using oriented single crystals, *Corrosion* 52 (1996) 453–464.
- [9] M.G. Alvarez, S.A. Fernandez, J.R. Galvele, Stress corrosion cracking in single crystals of Ag–Au alloy, *Corros. Sci.* 42 (2000) 739–752.
- [10] P. Arnoux, Atomistic simulations of stress corrosion cracking, *Corros. Sci.* 52 (2010) 1247–1257.
- [11] J.H. Driver, D. Jensen, N. Hansen, Large strain deformation structures in aluminium crystals with rolling texture orientations, *Acta Metall. Mater.* 42 (1994) 3105–3114.
- [12] A.V. Sameliuk, A.D. Vasilev, S.A. Firstov, Low temperature deformation and fracture behaviour of [1 0 0] and [1 1 0] chromium single crystals, *Inter. J. Refract. Met. Hard Mater.* 14 (1996) 249–255.
- [13] A. Sato, K. Kon, S. Tsujikawa, Y. Hisamatsu, Effect of crystallographic orientation on dissolution behavior of stainless steels single crystal, *Mater. Trans., JIM* 37 (1996) 729–732.
- [14] K. Kashiara, M. Tagami, F. Inoko, Deformed structure and crystal orientation at deformation bands in (0 1 1) aluminum single crystals, *Mater. Trans., JIM* 37 (1996) 564–571.
- [15] L.J. Qiao, X. Mao, J.L. Luo, Micromechanics of stress corrosion cracking of single-crystal austenitic type 321 stainless steel under mode II loading, *Corrosion* 52 (1996) 927–934.
- [16] P.A.S. Reed, P.H. Tucker, M.R. Joyce, Effects of mixed mode loading on fatigue and creep-fatigue in SRR-99 single crystals, *Mater. Sci. Eng.* A 394 (2005) 256–265.
- [17] A.L. Pilchak, A.H. Young, J.C. Williams, Stress corrosion cracking facet crystallography of Ti–8Al–1Mo–1V, *Corros. Sci.* 52 (2010) 3287–3296.
- [18] A.N. Stroh, The strength of Homer-Cottrell sessile dislocations, *Phil. Mag.* 1 (1956) 489–502.
- [19] T. Mimaki, Y. Nakazawa, S. Hashimoto, S. Miura, Stress corrosion cracking of copper bicrystals with (1 1 0)-Tilt  $\Sigma 3$ ,  $\Sigma 9$ , and  $\Sigma 11$  coincident site lattice boundaries, *Met. Trans.* A 21A (1990) 2355–2361.
- [20] E.I. Meletis, R.F. Hochman, The crystallography of stress corrosion cracking in face centered cubic single crystals, *Corros. Sci.* 24 (1984) 843–862.
- [21] J.I. Dickson, S. Li, J.-P. Bailon and D. Tromans, The fractography of transgranular SCC in F.C.C. metals, in Parkins Symposium on Fundamental Aspects of Stress Corrosion Cracking, in: S.M. Bruegger, E.I. Meletis, R.H. Jones, W.W. Gerberich, F.P. Ford, and R.W. Staehle (Eds.), TMS, Warrendale, PA. (1992) 303
- [22] T. Magnin, A. Chambreuil, B. Bayle, The corrosion-enhanced plasticity model for stress corrosion cracking in ductile fcc alloys, *Acta Mater.* 44 (1996) 1457–1470.
- [23] J.P. Chateau, D. Delafosse, T. Magnin, Numerical simulations of hydrogen-dislocation interactions in fcc stainless steels.: part II: hydrogen effects on crack tip plasticity at a stress corrosion crack, *Acta Mater.* 50 (2002) 1523–1538.
- [24] K. Sieradzki, R.C. Newman, Brittle behavior of ductile metals during stress-corrosion cracking, *Phil. Mag.* A 51 (1985) 95–132.
- [25] T. Magnin and J. Lepinoux, "Metallurgical aspects of the brittle SCC in austenitic stainless steels", in Parkins Symposium on Fundamental Aspects of Stress Corrosion Cracking, edited by S.M. Bruegger, E.I. Meletis, R.H. Jones, W.W. Gerberich, F.P. Ford, and R.W. Staehle, TMS, Warrendale, PA. (1992) 323.
- [26] Y. Yao, L.J. Qiao, A.A. Volinsky, Hydrogen effects on stainless steel passive film fracture studied by nanoindentation, *Corros. Sci.* 53 (2011) 2679–2683.
- [27] W.F. Flanagan, P. Bastias, B.D. Lichter, A theory of transgranular stress-corrosion cracking, *Acta Metall. Mater.* 39 (1991) 695–705.
- [28] T. Magnin, Environment sensitive fracture mechanisms, *Solid State Phenomena* 35–36 (1994) 319–334.
- [29] A. Chambreuil, J.P. Chateau, T. Magnin, Influence of the slip conditions on the stress corrosion cracking microprocesses in FCC materials, *Scripta Mater.* 37 (1997) 1337–1343.
- [30] J.F. Knott, *Fundamentals of Fracture Mechanics*, John Wiley & Sons Inc., New York 1973, p. 57.
- [31] A.A. Volinsky, N.R. Moody, M.L. Kottke, W.W. Gerberich, Fiducial mark and nanocrack zone formation during thin film delamination, *Phil. Mag.* 82 (2002) 3383–3391.
- [32] M.J. Lii, X.F. Chen, Y. Katz, W.W. Gerberich, Dislocation modeling and acoustic emission observation of alternating ductile/brittle events in Fe–3 wt%Si crystals, *Acta Metall. Mater.* 38 (1990) 2435–2453.
- [33] S.H. Chen, Y. Katz, W.W. Gerberich, Crack-tip strain fields and fracture microplasticity in hydrogen-induced cracking of Fe–3 wt% Si single crystals, *Phil. Mag.* A 63 (1991) 131–155.
- [34] W.W. Gerberich, T.J. Foecke, Hydrogen effects on material behavior, in: R. Moody, A.W. Thompson (Eds.), NACE, Houston, 1989, p. 687.
- [35] S.W. Dean, *Stress Corrosion – New Approaches*, ASTM, STP 610 (West Conshohocken, PA: ASTM, 1976), p. 308.
- [36] S.X. Gong, H. Horii, General solution to the problem of microcracks near the tip of a main crack, *J. Mech. Phys. Solids* 37 (1989) 27–46.